

CERN-PH-EP-2013-91  
May 30, 2013

## Hadron Transverse Momentum Distributions in Muon Deep Inelastic Scattering at 160 GeV/c

The COMPASS Collaboration

### Abstract

Multiplicities of charged hadrons produced in deep inelastic muon scattering off a  ${}^6\text{LiD}$  target have been measured as a function of the DIS variables  $x_{Bj}$ ,  $Q^2$ ,  $W^2$  and the final state hadron variables  $p_T$  and  $z$ . The  $p_T^2$  distributions are fitted with a single exponential function at low values of  $p_T^2$  to determine the dependence of  $\langle p_T^2 \rangle$  on  $x_{Bj}$ ,  $Q^2$ ,  $W^2$  and  $z$ . The  $z$ -dependence of  $\langle p_T^2 \rangle$  is shown to be a potential tool to extract the average intrinsic transverse momentum squared of partons,  $\langle k_{\perp}^2 \rangle$ , as a function of  $x_{Bj}$  and  $Q^2$  in a leading order QCD parton model.

*(to be submitted to European Physical Journal C)*

## The COMPASS Collaboration

C. Adolph<sup>8</sup>, M.G. Alekseev<sup>24</sup>, V.Yu. Alexakhin<sup>7</sup>, Yu. Alexandrov<sup>15,\*</sup>, G.D. Alexeev<sup>7</sup>, A. Amoroso<sup>27</sup>, V. Andrieux<sup>22</sup>, A. Austregesilo<sup>10,17</sup>, B. Badełek<sup>31</sup>, F. Balestra<sup>27</sup>, J. Barth<sup>4</sup>, G. Baum<sup>1</sup>, Y. Bedfer<sup>22</sup>, A. Berlin<sup>2</sup>, J. Bernhard<sup>13</sup>, R. Bertini<sup>27</sup>, K. Bicker<sup>10,17</sup>, J. Bieling<sup>4</sup>, R. Birsa<sup>24</sup>, J. Bisplinghoff<sup>3</sup>, M. Boer<sup>22</sup>, P. Bordalo<sup>12,a</sup>, F. Bradamante<sup>25</sup>, C. Braun<sup>8</sup>, A. Bravar<sup>24</sup>, A. Bressan<sup>25</sup>, M. Büchele<sup>9</sup>, E. Burtin<sup>22</sup>, L. Capozza<sup>22</sup>, M. Chiosso<sup>27</sup>, S.U. Chung<sup>17</sup>, A. Cicuttin<sup>26</sup>, M.L. Crespo<sup>26</sup>, S. Dalla Torre<sup>24</sup>, S.S. Dasgupta<sup>6</sup>, S. Dasgupta<sup>24</sup>, O.Yu. Denisov<sup>28</sup>, S.V. Donskov<sup>21</sup>, N. Doshita<sup>33</sup>, V. Duic<sup>25</sup>, W. Dünnweber<sup>16</sup>, M. Dziewiecki<sup>32</sup>, A. Efremov<sup>7</sup>, C. Elia<sup>25</sup>, P.D. Eversheim<sup>3</sup>, W. Eyrich<sup>8</sup>, M. Faessler<sup>16</sup>, A. Ferrero<sup>22</sup>, A. Filin<sup>21</sup>, M. Finger<sup>19</sup>, M. Finger jr.<sup>19</sup>, H. Fischer<sup>9</sup>, C. Franco<sup>12</sup>, N. du Fresne von Hohenesche<sup>13,10</sup>, J.M. Friedrich<sup>17</sup>, V. Frolov<sup>10</sup>, R. Garfagnini<sup>27</sup>, F. Gautheron<sup>2</sup>, O.P. Gavrichtchouk<sup>7</sup>, S. Gerassimov<sup>15,17</sup>, R. Geyer<sup>16</sup>, M. Giorgi<sup>25</sup>, I. Gnesi<sup>27</sup>, B. Gobbo<sup>24</sup>, S. Goertz<sup>4</sup>, S. Grabmüller<sup>17</sup>, A. Grasso<sup>27</sup>, B. Grube<sup>17</sup>, R. Gushterski<sup>7</sup>, A. Guskov<sup>7</sup>, T. Guthörl<sup>9,b</sup>, F. Haas<sup>17</sup>, D. von Harrach<sup>13</sup>, F.H. Heinsius<sup>9</sup>, F. Herrmann<sup>9</sup>, C. Heß<sup>2</sup>, F. Hinterberger<sup>3</sup>, Ch. Höppner<sup>17</sup>, N. Horikawa<sup>18,c</sup>, N. d'Hose<sup>22</sup>, S. Huber<sup>17</sup>, S. Ishimoto<sup>33,d</sup>, Yu. Ivanshin<sup>7</sup>, T. Iwata<sup>33</sup>, R. Jahn<sup>3</sup>, V. Jary<sup>20</sup>, P. Jasinski<sup>13</sup>, R. Joosten<sup>3</sup>, E. Kabuß<sup>13</sup>, D. Kang<sup>13</sup>, B. Ketzer<sup>17</sup>, G.V. Khaustov<sup>21</sup>, Yu.A. Khokhlov<sup>21,e</sup>, Yu. Kisselev<sup>2</sup>, F. Klein<sup>4</sup>, K. Klimaszewski<sup>30</sup>, J.H. Koivuniemi<sup>2</sup>, V.N. Kolosov<sup>21</sup>, K. Kondo<sup>33</sup>, K. Königsmann<sup>9</sup>, I. Konorov<sup>15,17</sup>, V.F. Konstantinov<sup>21</sup>, A.M. Kotzinian<sup>27</sup>, O. Kouznetsov<sup>7,22</sup>, M. Krämer<sup>17</sup>, Z.V. Kroumchtein<sup>7</sup>, N. Kuchinski<sup>7</sup>, F. Kunne<sup>22</sup>, K. Kurek<sup>30</sup>, R.P. Kurjata<sup>32</sup>, A.A. Lednev<sup>21</sup>, A. Lehmann<sup>8</sup>, S. Levorato<sup>25</sup>, J. Lichtenstadt<sup>23</sup>, A. Maggiora<sup>28</sup>, A. Magnon<sup>22</sup>, N. Makke<sup>22,25</sup>, G.K. Mallot<sup>10</sup>, A. Mann<sup>17</sup>, C. Marchand<sup>22</sup>, A. Martin<sup>25</sup>, J. Marzec<sup>32</sup>, H. Matsuda<sup>33</sup>, T. Matsuda<sup>14</sup>, G. Meshcheryakov<sup>7</sup>, W. Meyer<sup>2</sup>, T. Michigami<sup>33</sup>, Yu.V. Mikhailov<sup>21</sup>, Y. Miyachi<sup>33</sup>, A. Morreale<sup>22,f</sup>, A. Nagaytsev<sup>7</sup>, T. Nagel<sup>17</sup>, F. Nerling<sup>9</sup>, S. Neubert<sup>17</sup>, D. Neyret<sup>22</sup>, V.I. Nikolaenko<sup>21</sup>, J. Novy<sup>19</sup>, W.-D. Nowak<sup>9</sup>, A.S. Nunes<sup>12</sup>, A.G. Olshevsky<sup>7</sup>, M. Ostrick<sup>13</sup>, R. Panknin<sup>4</sup>, D. Panzieri<sup>29</sup>, B. Parsamyan<sup>27</sup>, S. Paul<sup>17</sup>, G. Piragino<sup>27</sup>, S. Platchkov<sup>22</sup>, J. Pochodzalla<sup>13</sup>, J. Polak<sup>11,25</sup>, V.A. Polyakov<sup>21</sup>, J. Pretz<sup>4,g</sup>, M. Quaresma<sup>12</sup>, C. Quintans<sup>12</sup>, J.-F. Rajotte<sup>16</sup>, S. Ramos<sup>12,a</sup>, G. Reicherz<sup>2</sup>, E. Rocco<sup>10</sup>, V. Rodionov<sup>7</sup>, E. Rondio<sup>30</sup>, N.S. Rossiyskaya<sup>7</sup>, D.I. Ryabchikov<sup>21</sup>, V.D. Samoylenko<sup>21</sup>, A. Sandacz<sup>30</sup>, M.G. Sapozhnikov<sup>7</sup>, S. Sarkar<sup>6</sup>, I.A. Savin<sup>7</sup>, G. Sbrizzai<sup>25</sup>, P. Schiavon<sup>25</sup>, C. Schill<sup>9</sup>, T. Schlüter<sup>16</sup>, A. Schmidt<sup>8</sup>, K. Schmidt<sup>9,b</sup>, L. Schmitt<sup>17,h</sup>, H. Schmüden<sup>3</sup>, K. Schönning<sup>10</sup>, S. Schopferer<sup>9</sup>, M. Schott<sup>10</sup>, O.Yu. Shevchenko<sup>7</sup>, L. Silva<sup>12</sup>, L. Sinha<sup>6</sup>, S. Sirtl<sup>9</sup>, M. Slunecka<sup>19</sup>, S. Sosio<sup>27</sup>, F. Sozzi<sup>24</sup>, A. Srnka<sup>5</sup>, L. Steiger<sup>24</sup>, M. Stolarski<sup>12</sup>, M. Sulc<sup>11</sup>, R. Sulej<sup>30</sup>, H. Suzuki<sup>33,c</sup>, P. Sznajder<sup>30</sup>, S. Takekawa<sup>28</sup>, J. Ter Wolbeek<sup>9,b</sup>, S. Tessaro<sup>24</sup>, F. Tessarotto<sup>24</sup>, F. Thibaud<sup>22</sup>, S. Uhl<sup>17</sup>, I. Uman<sup>16</sup>, M. Vandenbroucke<sup>22</sup>, M. Virius<sup>20</sup>, L. Wang<sup>2</sup>, T. Weisrock<sup>13</sup>, M. Wilfert<sup>13</sup>, R. Windmolders<sup>4</sup>, W. Wiślicki<sup>30</sup>, H. Wollny<sup>22</sup>, K. Zaremba<sup>32</sup>, M. Zavertyaev<sup>15</sup>, E. Zemlyanichkina<sup>7</sup>, N. Zhuravlev<sup>7</sup> and M. Ziembicki<sup>32</sup>

<sup>1</sup> Universität Bielefeld, Fakultät für Physik, 33501 Bielefeld, Germany<sup>i</sup>

<sup>2</sup> Universität Bochum, Institut für Experimentalphysik, 44780 Bochum, Germany<sup>i</sup>

<sup>3</sup> Universität Bonn, Helmholtz-Institut für Strahlen- und Kernphysik, 53115 Bonn, Germany<sup>i</sup>

<sup>4</sup> Universität Bonn, Physikalisches Institut, 53115 Bonn, Germany<sup>i</sup>

<sup>5</sup> Institute of Scientific Instruments, AS CR, 61264 Brno, Czech Republic<sup>j</sup>

<sup>6</sup> Matrivani Institute of Experimental Research & Education, Calcutta-700 030, India<sup>k</sup>

<sup>7</sup> Joint Institute for Nuclear Research, 141980 Dubna, Moscow region, Russia<sup>l</sup>

<sup>8</sup> Universität Erlangen–Nürnberg, Physikalisches Institut, 91054 Erlangen, Germany<sup>i</sup>

<sup>9</sup> Universität Freiburg, Physikalisches Institut, 79104 Freiburg, Germany<sup>i</sup>

<sup>10</sup> CERN, 1211 Geneva 23, Switzerland

<sup>11</sup> Technical University in Liberec, 46117 Liberec, Czech Republic<sup>j</sup>

<sup>12</sup> LIP, 1000-149 Lisbon, Portugal<sup>m</sup>

<sup>13</sup> Universität Mainz, Institut für Kernphysik, 55099 Mainz, Germany<sup>i</sup>

<sup>14</sup> University of Miyazaki, Miyazaki 889-2192, Japan<sup>n</sup>

- <sup>15</sup> Lebedev Physical Institute, 119991 Moscow, Russia
- <sup>16</sup> Ludwig-Maximilians-Universität München, Department für Physik, 80799 Munich, Germany<sup>io</sup>
- <sup>17</sup> Technische Universität München, Physik Department, 85748 Garching, Germany<sup>io</sup>
- <sup>18</sup> Nagoya University, 464 Nagoya, Japan<sup>n</sup>
- <sup>19</sup> Charles University in Prague, Faculty of Mathematics and Physics, 18000 Prague, Czech Republic<sup>j</sup>
- <sup>20</sup> Czech Technical University in Prague, 16636 Prague, Czech Republic<sup>j</sup>
- <sup>21</sup> State Research Center of the Russian Federation, Institute for High Energy Physics, 142281 Protvino, Russia
- <sup>22</sup> CEA IRFU/SPhN Saclay, 91191 Gif-sur-Yvette, France
- <sup>23</sup> Tel Aviv University, School of Physics and Astronomy, 69978 Tel Aviv, Israel<sup>p</sup>
- <sup>24</sup> Trieste Section of INFN, 34127 Trieste, Italy
- <sup>25</sup> University of Trieste, Department of Physics and Trieste Section of INFN, 34127 Trieste, Italy
- <sup>26</sup> Abdus Salam ICTP and Trieste Section of INFN, 34127 Trieste, Italy
- <sup>27</sup> University of Turin, Department of Physics and Torino Section of INFN, 10125 Turin, Italy
- <sup>28</sup> Torino Section of INFN, 10125 Turin, Italy
- <sup>29</sup> University of Eastern Piedmont, 15100 Alessandria, and Torino Section of INFN, 10125 Turin, Italy
- <sup>30</sup> National Centre for Nuclear Research, 00-681 Warsaw, Poland<sup>q</sup>
- <sup>31</sup> University of Warsaw, Faculty of Physics, 00-681 Warsaw, Poland<sup>q</sup>
- <sup>32</sup> Warsaw University of Technology, Institute of Radioelectronics, 00-665 Warsaw, Poland<sup>q</sup>
- <sup>33</sup> Yamagata University, Yamagata, 992-8510 Japan<sup>n</sup>
- <sup>a</sup> Also at IST, Universidade Técnica de Lisboa, Lisbon, Portugal
- <sup>b</sup> Supported by the DFG Research Training Group Programme 1102 “Physics at Hadron Accelerators”
- <sup>c</sup> Also at Chubu University, Kasugai, Aichi, 487-8501 Japan<sup>n</sup>
- <sup>d</sup> Also at KEK, 1-1 Oho, Tsukuba, Ibaraki, 305-0801 Japan
- <sup>e</sup> Also at Moscow Institute of Physics and Technology, Moscow Region, 141700, Russia
- <sup>f</sup> present address: National Science Foundation, 4201 Wilson Boulevard, Arlington, VA 22230, United States
- <sup>g</sup> present address: RWTH Aachen University, III. Physikalisches Institut, 52056 Aachen, Germany
- <sup>h</sup> Also at GSI mbH, Planckstr. 1, D-64291 Darmstadt, Germany
- <sup>i</sup> Supported by the German Bundesministerium für Bildung und Forschung
- <sup>j</sup> Supported by Czech Republic MEYS Grants ME492 and LA242
- <sup>k</sup> Supported by SAIL (CSR), Govt. of India
- <sup>l</sup> Supported by CERN-RFBR Grants 08-02-91009
- <sup>m</sup> Supported by the Portuguese FCT - Fundação para a Ciência e Tecnologia, COMPETE and QREN, Grants CERN/FP/109323/2009, CERN/FP/116376/2010 and CERN/FP/123600/2011
- <sup>n</sup> Supported by the MEXT and the JSPS under the Grants No.18002006, No.20540299 and No.18540281; Daiko Foundation and Yamada Foundation
- <sup>o</sup> Supported by the DFG cluster of excellence ‘Origin and Structure of the Universe’ ([www.universe-cluster.de](http://www.universe-cluster.de))
- <sup>p</sup> Supported by the Israel Science Foundation, founded by the Israel Academy of Sciences and Humanities
- <sup>q</sup> Supported by the Polish NCN Grant DEC-2011/01/M/ST2/02350
- \* Deceased

## 1 Introduction

Semi-Inclusive measurements of Deep Inelastic Scattering (SIDIS) of leptons off nucleons provide information about the partonic structure of the nucleon and the hadronization of partons, and hence offer a wide testing ground of Quantum Chromodynamics (QCD). Subject of the present study are the transverse momentum distributions of charged hadrons produced in the current fragmentation region in lepton-nucleon scattering off unpolarised nucleons. The hadron transverse momentum  $p_T$  is defined with respect to the virtual photon direction. The following standard notations are used:  $\ell$  and  $\ell'$  for the incoming and outgoing lepton,  $N$  for the target nucleon,  $h$  for the outgoing hadron and  $X$  for the unobserved particles in the final state;  $l, l', P$ , and  $p$  denote the 4-momenta of  $\ell, \ell', N$ , and  $h$ . The general expression for the differential SIDIS cross section describing the reaction  $\ell + N \rightarrow \ell' + h + X$  in the one-photon approximation is [1, 2]:

$$\frac{d^5 \sigma^h(x_{Bj}, Q^2, z, p_T^2, \phi_h)}{dx_{Bj} dQ^2 dz dp_T^2 d\phi_h} = \frac{d^4 \sigma^h(x_{Bj}, Q^2, z, p_T^2)}{2\pi dx_{Bj} dQ^2 dz dp_T^2} \left( 1 + a_1(x_{Bj}, Q^2, z, p_T^2) \cos \phi_h + a_2(x_{Bj}, Q^2, z, p_T^2) \cos 2\phi_h + \lambda a_3(x_{Bj}, Q^2, z, p_T^2) \sin \phi_h \right). \quad (1)$$

Here,  $\lambda$  is the helicity of the incoming lepton and the standard SIDIS variables are used: the 4-momentum transfer  $q = (l - l')$ , the photon virtuality  $Q^2 = -q^2$ , the Bjorken scaling variable  $x_{Bj} = Q^2/2P \cdot q$ , the hadron fractional energy  $z = P \cdot p/P \cdot q$  and the azimuthal angle  $\phi_h$  of the transverse momentum of the hadron with respect to the lepton scattering plane around the virtual photon direction. After integration over  $\phi_h$ , the cross section does not depend on the initial lepton polarisation  $\lambda$ . The hadron multiplicity per interaction is defined as the ratio of the differential SIDIS cross section over the differential DIS cross section  $d^2 \sigma^{DIS}(x_{Bj}, Q^2)/dx_{Bj} dQ^2$ . Thus, the differential hadron multiplicity,  $d^2 n^h/dz dp_T^2$ , depends on four variables,  $x_{Bj}, Q^2, z, p_T^2$ :

$$\frac{d^2 n^h(x_{Bj}, Q^2, z, p_T^2)}{dz dp_T^2} = \frac{d^4 \sigma^h(x_{Bj}, Q^2, z, p_T^2)/(dx_{Bj} dQ^2 dz dp_T^2)}{d^2 \sigma^{DIS}(x_{Bj}, Q^2)/(dx_{Bj} dQ^2)}. \quad (2)$$

Within a pQCD Leading Order (LO) parton model the shape of the  $p_T^2$  distributions depends on the intrinsic transverse momentum  $k_\perp$  of the partons and the transverse momentum of the hadrons  $p_\perp$  acquired during parton fragmentation. The amount of the contributions of  $k_\perp$  and  $p_\perp$  may depend on the hadron type, parton flavour, and on kinematic variables such as  $x_{Bj}, Q^2$  and  $z$ . Already in the 1970s, SIDIS was understood as a tool to access the intrinsic transverse momentum of the partons (see e.g. [3] and references therein). The connection between the intrinsic transverse momenta of the parton  $k_\perp$  and that of the hadron  $p_\perp$  and the measured transverse momentum  $p_T$  of the produced hadron is illustrated in Fig. 1, assuming single photon exchange and leading order pQCD.

During the last three decades significant efforts, both in experimental and theoretical studies of (polarised) SIDIS, have been undertaken. Currently this process is considered to be one of the most promising to study the hadronization process and also the spin-dependent three-dimensional structure of the nucleon (see, e.g. [4]). Recently, a complete QCD treatment of transverse momentum and spin-dependent SIDIS was presented in Ref. [5] where factorization was derived in terms of well defined unintegrated or Transverse Momentum Dependent parton distribution and fragmentation functions (TMDs) with individual hard scale evolution properties. This formalism has been applied in Ref. [6] to obtain the  $Q^2$  evolution of unpolarised TMDs; a mandatory information needed for a correct comparison of data measured in experiments at different hard scales [4].

Hadron leptoproduction has been studied by many experiments. Some recent examples are: JLab [7], HERMES [8] and E665 [9]. Earlier, EMC [10] covered most of the kinematic range of COMPASS. However, COMPASS has collected much more data in this range and the statistical errors of the present

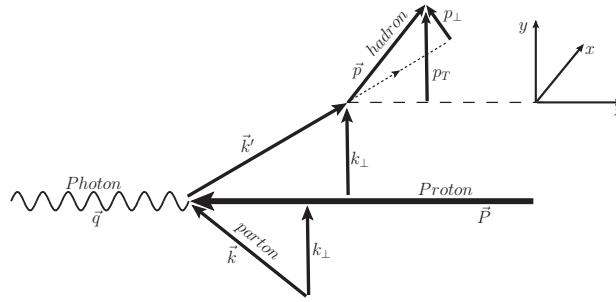


Fig. 1: Sketch showing the kinematic variables for the absorption of a virtual photon by a parton with intrinsic transverse momentum  $k_{\perp}$  and the subsequent hadronization. The transverse momentum of the observed hadron is denoted by  $p_T$  when defined with respect to the virtual photon direction in the photon nucleon center of mass system and by  $p_{\perp}$  when defined with respect to the scattered parton direction.

analysis are therefore significantly smaller, although only part of the available data has been used. The results presented here are obtained from data taken during the year 2004. More details of the analysis are described in Ref. [11].

## 2 Experiment, Data Selection and Acceptance

The COMPASS experiment is installed on the M2 beam line of the CERN SPS [12]. Polarised 160 GeV/ $c$  muons with an intensity of  $2 \times 10^8 \mu/\text{spill}$  (one spill of 4.8 s length per 16.8 s) and a polarisation of 80% are scattered off a longitudinally polarised  ${}^6\text{LiD}$  target. In 2004 the target consisted of two cells with opposite polarisation which was reversed every 8 hours. It has been verified that summing up the data from both cells yields a data sample with vanishing polarisation for the present analysis. The COMPASS detector is a large acceptance two-stage spectrometer which covers the kinematic range from quasi-real photoproduction to DIS. Both stages are equipped with hadron calorimeters and use absorber walls for muon identification. Charged particles emerging from the primary interaction vertex in the forward direction are identified as muons if they traverse at least 30 radiation length, otherwise they are identified as hadrons. The selection requires reconstructed trajectories in the detectors situated upstream and downstream of the first magnet. This ensures that the track momentum and sign of charge are well defined by bending in the magnetic field. The COMPASS ability to separate pions, kaons and protons with a Ring Imaging Cherenkov detector was not used in this analysis. Muon interactions with  $Q^2 > 1.0$  (GeV/ $c$ )<sup>2</sup> and  $0.1 < y < 0.9$  are selected, where  $y = \nu/E_{\mu}$ , and  $\nu = E_{\mu} - E_{\mu'}$  is the difference between the laboratory energies of the incoming and outgoing muon  $\mu$  and  $\mu'$ . With the above selection, the hadronic energy squared  $W^2 = 2M\nu + M^2 - Q^2$  is  $> 25$  GeV/ $c$ , above the nucleon resonance region. Here,  $M$  is the nucleon mass. The total number of inclusive events selected for this analysis is  $45.8 \times 10^6$ , corresponding to an integrated luminosity of  $775 \text{ pb}^{-1}$ . The events are sampled into 23 intervals in  $Q^2$  from 1 to 10 (GeV/ $c$ )<sup>2</sup> and  $x_{Bj}$  from 0.004 to 0.12, as shown in Fig. 2. The ranges and average values of  $Q^2$  and  $x_{Bj}$  are shown in Tab. 1. Each of these  $(x_{Bj}, Q^2)$  intervals is further subdivided into 8 intervals in  $z$  from 0.2 to 0.8.

In order to correct for event losses caused by the non uniform acceptance of the COMPASS spectrometer, a full Monte Carlo (MC) simulation has been performed. The events were generated with LEPTO [13], passed through the spectrometer with a GEANT [14] based simulation program and reconstructed with the reconstruction software as the real data events.

The SIDIS acceptances  $A_{SIDIS}^{(+,-)}$  for detecting, together with the scattered muon, a positive ( $h^+$ ) or negative hadrons ( $h^-$ ) respectively factorize in an inclusive muon acceptance  $A_{incl}(Q^2, y)$  and a positive or negative hadron acceptance  $A_{h^{+,-}}(^{lab}p_T, ^{lab}\eta)$ . These acceptances depend on the spectrometer charac-

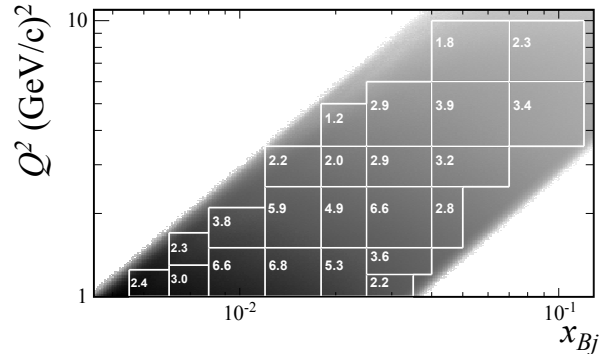


Fig. 2: Event distribution in the inclusive variables  $Q^2$  and  $x_{Bj}$  and the 23 bins of the hadron cross section analysis. Within each bin, the fraction of events contained is indicated in %.

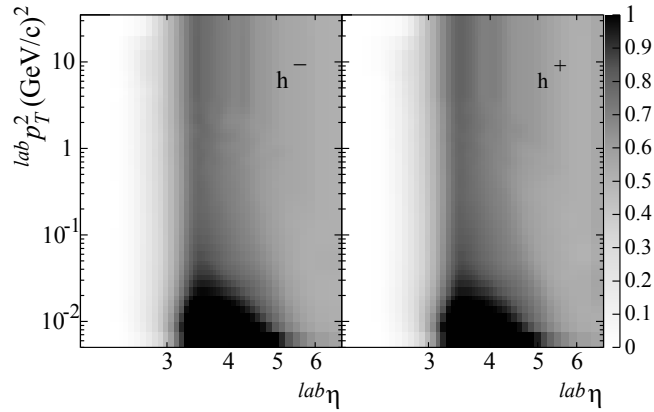


Fig. 3: Hadron acceptances  $A_{h^-}$  and  $A_{h^+}$  determined with the Monte Carlo simulation for  $Q^2 > 1$   $(\text{GeV}/c)^2$  as a function of  ${}^{lab}p_T$  and  ${}^{lab}\eta$  for negative hadrons  $h^-$  (left) and positive hadrons  $h^+$  (right). The acceptances have been smoothed in order to reduce the granularity from the binning.

teristics, making the use of variables defined in the laboratory frame preferable; therefore, the transverse momentum  ${}^{lab}p_T$ , the polar angle  ${}^{lab}\theta$ , and the pseudorapidity  ${}^{lab}\eta = -\ln(\tan \frac{{}^{lab}\theta}{2})$  of the hadron are defined with respect to the direction of the incoming muon. The choice of  ${}^{lab}\theta$  is particularly convenient to exhibit the acceptance cut due to the aperture limit of the polarised target magnet at  ${}^{lab}\theta = 70$  mrad for the upstream edge of the target. The factorization of hadron and muon acceptances implies that the differential multiplicities only depend on  $A_{h^{(+, -)}}$  since  $A_{incl}$  cancels, see Eq. 2. Figure 3 shows the hadron acceptances  $A_{h^-}$  and  $A_{h^+}$  used in the analysis.

The four-dimensional acceptance used in the present analysis is integrated over the azimuthal angle of the hadrons, i.e. does not take into account the azimuthal modulations in the cross section [2]. The systematic effect on the extracted  $\langle p_T^2 \rangle$  have been investigated and found to be negligible.

### 3 Results

The differential multiplicities  $d^2n^{h^\pm}/dzdp_T^2$  in bins of  $(Q^2, x_{Bj})$  are defined in the introduction in terms of the semi-inclusive and inclusive differential cross sections. They are obtained as the acceptance corrected number of hadrons  $\Delta^4 N^{h^\pm}$  in  $8 \times 40$  ( $z, p_T^2$ ) bins and 23  $(\Delta x_{Bj}, \Delta Q^2)$  bins, divided by the number  $\Delta^2 N^\mu$

Bin	$x_{bj}^{min}$	$x_{bj}^{max}$	$\langle x_{bj} \rangle$	$Q_{min}^2$	$Q_{max}^2$	$\langle Q^2 \rangle$
1	0.0045	0.0060	0.0052	1.0	1.25	1.11
2	0.0060	0.0080	0.0070	1.0	1.30	1.14
3	0.0060	0.0080	0.0070	1.3	1.70	1.48
4	0.0080	0.0120	0.0099	1.0	1.50	1.22
5	0.0080	0.0120	0.0099	1.5	2.10	1.76
6	0.0120	0.0180	0.0148	1.0	1.50	1.22
7	0.0120	0.0180	0.0148	1.5	2.50	1.92
8	0.0120	0.0180	0.0150	2.5	3.50	2.90
9	0.0180	0.0250	0.0213	1.0	1.50	1.23
10	0.0180	0.0250	0.0213	1.5	2.50	1.92
11	0.0180	0.0250	0.0213	2.5	3.50	2.94
12	0.0180	0.0250	0.0216	3.5	5.00	4.07
13	0.0250	0.0350	0.0295	1.0	1.20	1.10
14	0.0250	0.0400	0.0316	1.2	1.50	1.34
15	0.0250	0.0400	0.0318	1.5	2.50	1.92
16	0.0250	0.0400	0.0319	2.5	3.50	2.95
17	0.0250	0.0400	0.0323	3.5	6.00	4.47
18	0.0400	0.0500	0.0447	1.5	2.50	1.93
19	0.0400	0.0700	0.0533	2.5	3.50	2.95
20	0.0400	0.0700	0.0536	3.5	6.00	4.57
21	0.0400	0.0700	0.0550	6.0	10.0	7.36
22	0.0700	0.1200	0.0921	3.5	6.00	4.62
23	0.0700	0.1200	0.0932	6.0	10.0	7.57

Table 1: Definition of the 23 bins of  $x_{bj}$  and  $Q^2$  and corresponding mean values;  $Q^2$  is in units of  $(\text{GeV}/c)^2$ .

of muon interactions in the same  $(\Delta x_{Bj}, \Delta Q^2)$  bins:

$$\frac{d^2 n^{h\pm}(z, p_T^2, x_{Bj}, Q^2)}{dz dp_T^2} \Big|_{\Delta x_{Bj} \Delta Q^2} \approx \frac{\Delta^4 N^{h\pm}(z, p_T^2, x_{Bj}, Q^2) / (\Delta z \Delta p_T^2 \Delta x_{Bj} \Delta Q^2)}{\Delta^2 N^\mu(x_{Bj}, Q^2) / (\Delta x_{Bj} \Delta Q^2)}. \quad (3)$$

The distributions for two selected  $(Q^2, x_{Bj})$  bins are shown in Fig. 4 for all  $z$  intervals. The full data set, including more  $p_T^2$  bins, is available on HEPDATA [15]. As can be seen from Eq. 3 the uncertainty of the integrated luminosity cancels and the only contributions to systematic uncertainties of the multiplicities come from the hadron acceptance and the assumption of factorization of hadron and muon acceptance. The total systematic uncertainty due to acceptance has been estimated to be 5% [11]. Only statistical errors are shown in the figures.

The fits are performed at values of  $p_T$  smaller than 0.85  $\text{GeV}/c$  to stay away from pQCD effects where the assumption of a simple exponential distribution is known to fail [16, 17] and at  $p_T$  larger than 0.1  $\text{GeV}/c$  to exclude a region where the experimental resolution may affect the distribution. In this range, the  $p_T^2$  distributions are fitted with a single exponential functions  $Ae^{-p_T^2/\langle p_T^2 \rangle}$  to extract the inverse slope  $\langle p_T^2 \rangle$ . The values of  $\langle p_T^2 \rangle$  for all intervals of  $x_{Bj}$ ,  $Q^2$  and  $z$  are shown in Figs. 5 and 6 and in Tabs. 2 and 3. These figures and tables contain the basic experimental information extracted from the fits of the  $p_T^2$  distributions.

In Fig. 7 the dependence of the fitted  $\langle p_T^2 \rangle$  on  $x_{Bj}$  is shown for a low- $z$  and a high- $z$  bin and for a low- and a high- $Q^2$  bin. At higher  $z$  the positive hadrons clearly have higher  $\langle p_T^2 \rangle$  than the negative hadrons. For hadrons with lower  $z$  however, no difference is observed in the  $p_T^2$  distributions. A similar behaviour was already reported by HERMES [21] for the average  $p_T^2$ , not determined by a fit but from a standard average

$Q^2, x_{B,j}$ Bin	$z$ bins $\rightarrow$							
	0.2÷0.25	0.25÷0.3	0.3÷0.35	0.35÷0.4	0.4÷0.5	0.5÷0.6	0.6÷0.7	0.7÷0.8
1	.2254(13)	.2394(17)	.2607(23)	.2738(30)	.2981(31)	.3072(43)	.3299(65)	.2674(57)
2	.2241(10)	.2457(14)	.2614(19)	.2763(24)	.2952(24)	.3060(35)	.3009(44)	.2650(46)
3	.2234(13)	.2390(18)	.2631(24)	.2761(31)	.2986(32)	.3327(52)	.3348(69)	.2985(68)
4	.2239(6)	.2424(9)	.2592(12)	.2738(15)	.2915(15)	.3006(21)	.3087(29)	.2670(30)
5	.2270(9)	.2438(13)	.2634(17)	.2777(22)	.3073(24)	.3387(38)	.3419(51)	.2998(55)
6	.2231(6)	.2442(8)	.2610(11)	.2755(14)	.2914(13)	.3053(19)	.3010(25)	.2677(27)
7	.2246(7)	.2418(9)	.2641(13)	.2779(17)	.3013(17)	.3338(27)	.3410(38)	.3105(44)
8	.2250(13)	.2470(18)	.2723(25)	.2893(33)	.3338(38)	.3829(67)	.420(11)	.447(17)
9	.2122(7)	.2408(9)	.2630(12)	.2762(15)	.2953(15)	.3087(21)	.3094(26)	.2699(27)
10	.2222(7)	.2439(10)	.2617(13)	.2806(17)	.3034(17)	.3347(28)	.3309(37)	.2946(39)
11	.2250(12)	.2425(16)	.2667(22)	.2886(30)	.3243(34)	.3642(57)	.3912(88)	.3485(95)
12	.2289(17)	.2530(24)	.2828(35)	.3031(48)	.3515(55)	.421(11)	.417(14)	.538(34)
13	.1766(13)	.2020(15)	.2299(18)	.2597(23)	.2909(22)	.3003(29)	.2956(34)	.2704(37)
14	.1866(9)	.2171(13)	.2436(15)	.2640(18)	.2893(17)	.3131(24)	.3099(30)	.2758(31)
15	.2078(6)	.2355(8)	.2577(11)	.2759(14)	.3050(14)	.3319(22)	.3364(29)	.3025(31)
16	.2229(9)	.2441(13)	.2678(18)	.2882(23)	.3230(26)	.3587(42)	.3749(59)	.3395(69)
17	.2257(10)	.2493(14)	.2761(20)	.3064(28)	.3468(32)	.4050(59)	.4321(91)	.384(10)
18	.1799(11)	.2063(13)	.2340(17)	.2500(19)	.2853(20)	.3197(30)	.3321(40)	.2984(42)
19	.1944(9)	.2245(12)	.2486(15)	.2735(20)	.3088(22)	.3434(34)	.3656(49)	.3609(62)
20	.2167(8)	.2415(11)	.2700(15)	.2947(21)	.3370(23)	.3959(42)	.4170(63)	.3994(76)
21	.2311(13)	.2579(18)	.2908(27)	.3178(37)	.3588(41)	.4307(80)	.490(14)	.507(21)
22	.1738(10)	.1990(12)	.2319(16)	.2578(21)	.2969(22)	.3437(38)	.3809(57)	.3809(74)
23	.2091(10)	.2448(15)	.2714(21)	.2989(28)	.3441(31)	.4072(57)	.470(10)	.469(13)

Table 2: Fitted  $\langle p_T^2 \rangle$  in units of  $(\text{GeV}/c)^2$  for the 23  $(x_{B,j}, Q^2)$  bins (rows) and the 8  $z$  intervals (columns) for positive hadrons. The error of the least significant digit(s) is given in parentheses. Same information as Fig. 5



Bin	0.2 ÷ 0.25	0.25 ÷ 0.3	0.3 ÷ 0.35	0.35 ÷ 0.4	0.4 ÷ 0.5	0.5 ÷ 0.6	0.6 ÷ 0.7	0.7 ÷ 0.8
1	.2285(13)	.2472(18)	.2606(24)	.2651(29)	.2741(27)	.2699(35)	.2551(41)	.2259(42)
2	.2241(10)	.2450(15)	.2607(20)	.2713(25)	.2793(23)	.2806(31)	.2697(37)	.2297(37)
3	.2305(14)	.2510(19)	.2690(25)	.2802(33)	.2843(30)	.2851(40)	.2778(50)	.2562(54)
4	.2254(7)	.2448(9)	.2614(13)	.2719(16)	.2814(15)	.2836(20)	.2700(24)	.2375(26)
5	.2276(10)	.2498(14)	.2666(19)	.2752(23)	.2987(24)	.3056(33)	.2990(42)	.2722(46)
6	.2216(7)	.2431(9)	.2604(12)	.2766(15)	.2869(14)	.2870(19)	.2780(24)	.2297(23)
7	.2260(7)	.2498(10)	.2653(14)	.2823(18)	.2989(18)	.3171(27)	.3068(35)	.2657(37)
8	.2346(14)	.2555(19)	.2841(28)	.2976(36)	.3233(38)	.3572(62)	.3674(88)	.328(10)
9	.2071(8)	.2326(10)	.2540(13)	.2686(16)	.2837(15)	.2888(20)	.2767(24)	.2316(24)
10	.2219(8)	.2440(11)	.2646(14)	.2831(19)	.2992(19)	.3150(28)	.3068(36)	.2596(35)
11	.2331(13)	.2512(18)	.2742(25)	.2953(34)	.3243(37)	.3578(62)	.3587(85)	.3048(87)
12	.2333(18)	.2644(27)	.2908(40)	.3057(50)	.3443(58)	.383(10)	.417(16)	.379(18)
13	.1669(12)	.1933(16)	.2201(20)	.2400(23)	.2614(21)	.2640(27)	.2457(29)	.2083(28)
14	.1835(11)	.2086(12)	.2302(15)	.2536(19)	.2693(18)	.2794(24)	.2648(27)	.2240(26)
15	.2067(7)	.2316(9)	.2548(12)	.2728(15)	.2976(16)	.3081(22)	.3015(27)	.2492(26)
16	.2219(10)	.2482(14)	.2652(19)	.2907(26)	.3254(29)	.3541(47)	.3473(62)	.2971(60)
17	.2325(11)	.2556(16)	.2844(23)	.3092(31)	.3506(37)	.4033(68)	.3890(87)	.3432(95)
18	.1746(11)	.1994(14)	.2232(18)	.2411(21)	.2692(21)	.2850(30)	.2882(38)	.2394(35)
19	.1915(9)	.2193(13)	.2452(18)	.2715(23)	.3040(25)	.3268(39)	.3319(51)	.2869(52)
20	.2163(9)	.2456(12)	.2765(18)	.3007(25)	.3389(28)	.3703(45)	.3909(70)	.3382(73)
21	.2370(14)	.2686(21)	.2994(31)	.3246(44)	.3744(53)	.4235(96)	.414(13)	.391(17)
22	.1730(10)	.1967(13)	.2314(19)	.2623(27)	.2867(26)	.3218(41)	.3598(66)	.3310(75)
23	.2166(13)	.2482(17)	.2814(25)	.3050(35)	.3531(41)	.3976(71)	.414(11)	.388(13)

Table 3: Fitted  $\langle p_T^2 \rangle$  in units of  $(\text{GeV}/c)^2$  for the 23 ( $x_{Bj}$ ,  $Q^2$ ) bins (rows) and the 8  $z$  intervals (columns) for negative hadrons. The error of the least significant digit(s) is given in parentheses. Same information as Fig. 6

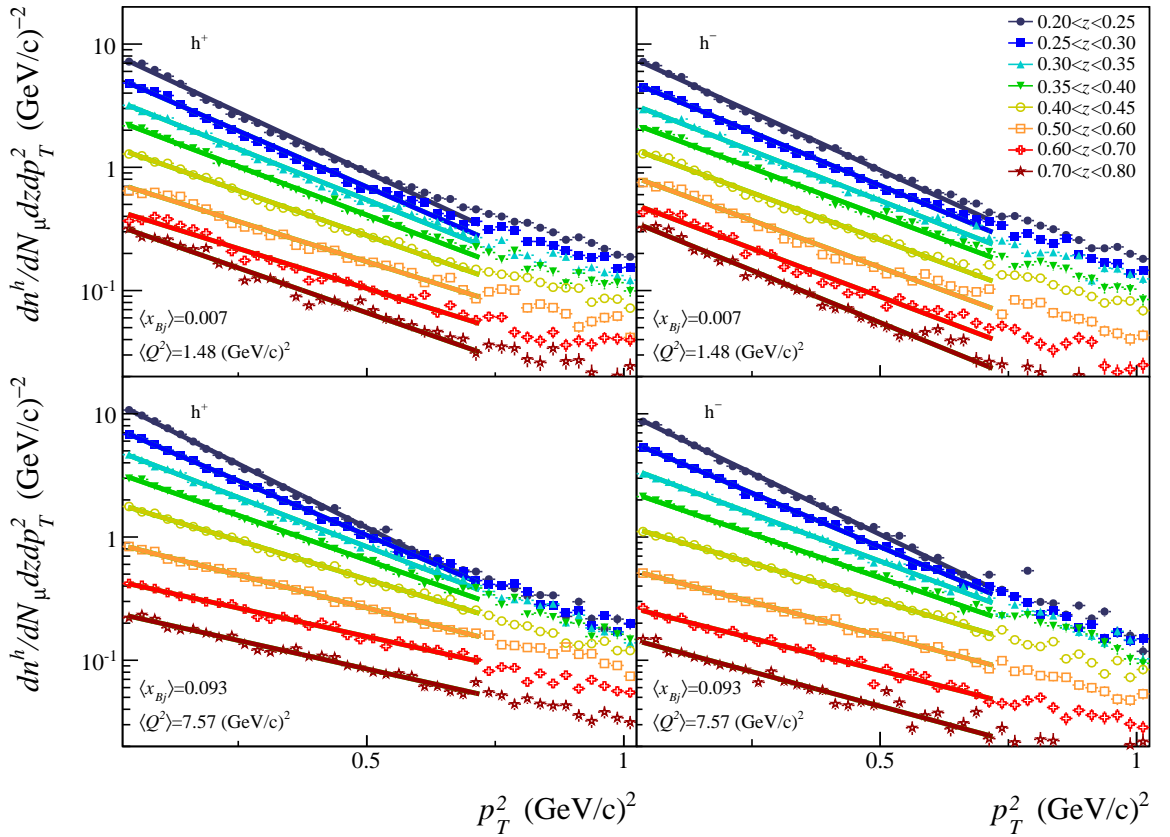


Fig. 4: The  $p_T^2$  dependence of the differential multiplicities  $d^2n^h/dzdp_T^2$  of positive hadrons (left) and negative hadrons (right) fitted by an exponential for  $1 < Q^2 \text{ (GeV/c)}^2 < 1.5$ ,  $0.006 < x_{Bj} < 0.008$  (top) and  $6 < Q^2 \text{ (GeV/c)}^2 < 10$ ,  $0.07 < x_{Bj} < 0.12$  (bottom) subdivided into eight  $z$  intervals, see legend of upper pictures. The average values  $\langle Q^2 \rangle$  and  $\langle x_{Bj} \rangle$  for the chosen  $(Q^2, x_{Bj})$  intervals are indicated in the pictures. The systematic error of 5% is not included in the errors.

over the entire  $p_T$  range, i.e.  $\langle p_T^2 \rangle_{all}$ . The  $z$ -dependence as well as the hadron charge dependence of the  $p_T^2$  distributions will be further investigated below and is related to the intrinsic transverse momentum of the partons.

It is interesting to compare the values and  $W^2$ -dependence of  $\langle p_T^2 \rangle$  obtained from the fit at small  $p_T$  with the values and  $W^2$ -dependence of  $\langle p_T^2 \rangle_{all}$ . The  $W^2$ -dependence of  $\langle p_T^2 \rangle$ , obtained from the fit in the bin  $0.5 < z < 0.6$  is shown in Fig. 8, that one of  $\langle p_T^2 \rangle_{all}$  in Fig. 9. In addition to the data points, Fig. 9 shows lines, which represent fits of the data points assuming a linear function of  $\ln W^2$ . Because of the  $Q^2$ -dependence, the last points are somewhat below the fit. The authors of Ref. [18] first suggested that  $\langle p_T^2 \rangle_{all}$  should depend linearly on the  $\mu N$  center of mass energy squared  $s$ . They have verified their prediction with results from three fixed target experiments: JLab, HERMES and COMPASS, see Fig. 10. Fig. 10a shows the  $p_T^2$  distribution of charged hadrons with  $0.5 < z < 0.6$  and integrated over  $Q^2$  and  $x_{Bj}$ , measured by COMPASS, which was used to determine the acceptance corrected  $\langle p_T^2 \rangle_{all}$ . Fig. 10b taken from Ref. [18] shows the dependence of  $\langle p_T^2 \rangle_{all}$  on  $s$ . Their value for COMPASS, represented by the black dots, was not corrected for acceptance. The new, acceptance corrected COMPASS value  $\langle p_T^2 \rangle_{all}$  added to Fig. 10b (red dot) is shown in a recent paper [19], and used to quantify the  $p_T$  broadening [20] in a model to determine the Sivers and Boer-Mulders asymmetries at COMPASS and HERMES. The result of the model of Pasquini and Schweitzer was closer to the COMPASS data when  $p_T$  broadening is included. The authors of Ref. [18] also note that  $\langle p_T^2 \rangle_{all}$  may depend linearly on  $W^2$  rather than  $s$ .

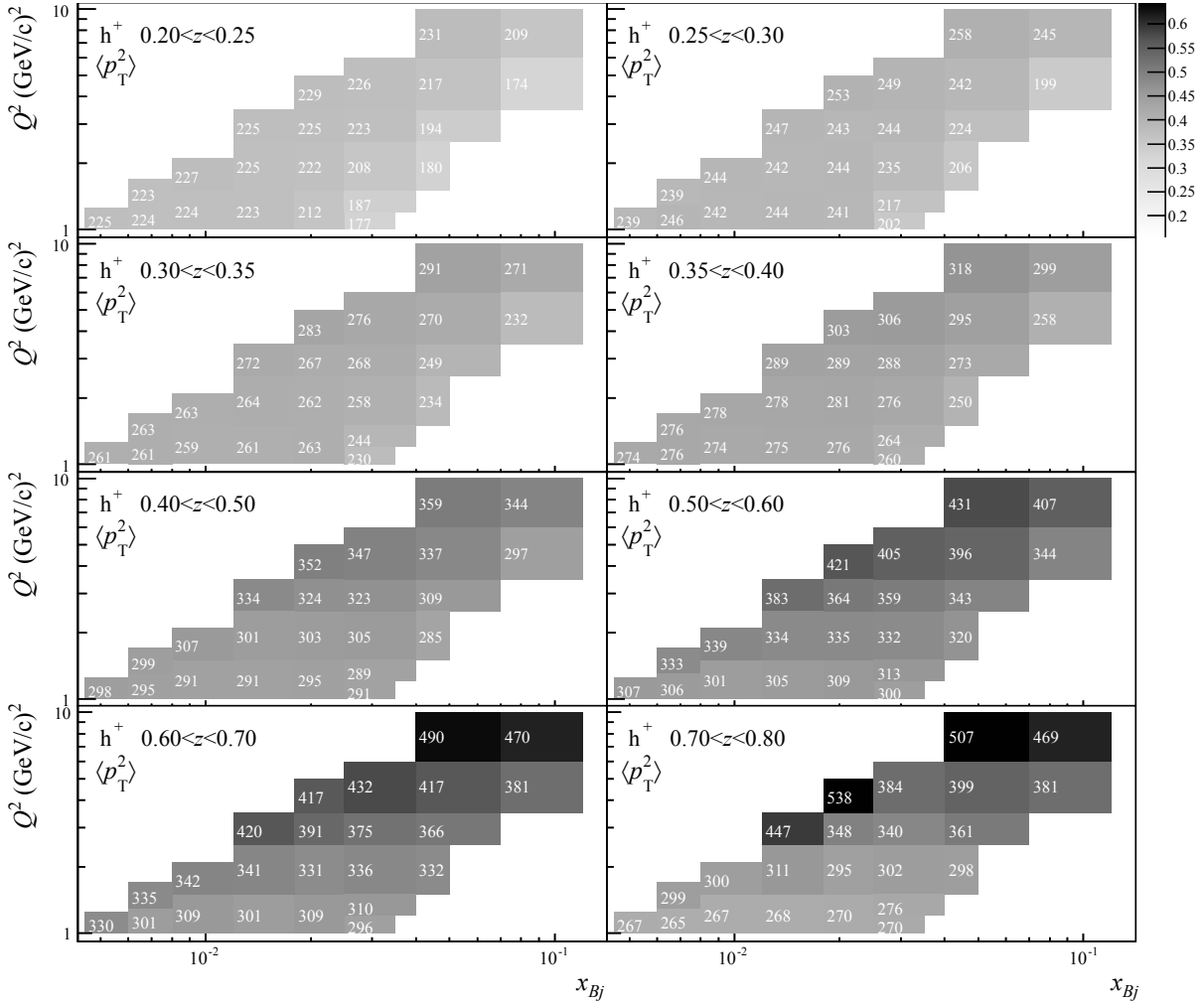


Fig. 5: Fitted  $\langle p_T^2 \rangle$  vs  $(x_{Bj}, Q^2)$  for all  $z$  intervals for positive hadrons. The values are both written inside each interval and shown as a gray scale. The same gray scale is used for all the plots. The written values are in units of  $(\text{GeV}/c)^2 \times 1000$ .

However, the dependence shown in Fig. 9 is more compatible with a linear dependence on  $\ln W^2$  as was found by several experiments (see, e.g. [10]). The relation is not well established and, as mentioned in Ref. [18], the linear dependence on  $s$  for Drell-Yan which inspired their SIDIS prediction, could also be a linear dependence on  $\sqrt{s}$ . Contrary to the case of  $\langle p_T^2 \rangle_{all}$  in Fig. 9, the  $W^2$ -dependence of the fitted  $\langle p_T^2 \rangle$  shown in Fig. 8 is much weaker, as expected, since  $\langle p_T^2 \rangle$  is assumed to be unaffected by pQCD, as opposed to  $\langle p_T^2 \rangle_{all}$ .

Another interesting observable is the ratio of the multiplicities of positive and negative hadrons integrated over  $p_T^2$  and  $Q^2$ . The hadron multiplicity ratios are shown in Fig. 11 and compared with previous data taken by the EMC experiment [10]. COMPASS results show clearly the  $z$ - and  $x_{Bj}$ -dependence, where the fraction of positive hadrons increases with  $x_{Bj}$  (getting closer to the valence region) and  $z$  (more related to the energy of the struck parton). This behaviour can be qualitatively connected with the fact that the positive valence quarks have a larger electric charge than the negative ones.

The  $z^2$ -dependence of the fitted  $\langle p_T^2 \rangle$  is of particular interest. There are theoretical predictions allowing the extraction of the intrinsic transverse momenta  $k_\perp$  and  $p_\perp$  from this  $z^2$ -dependence [16]. At leading order QCD, assuming single photon exchange and an independent fragmentation process, the hadron muoproduction cross section can be expressed in terms of a hard muon-parton interaction cross section

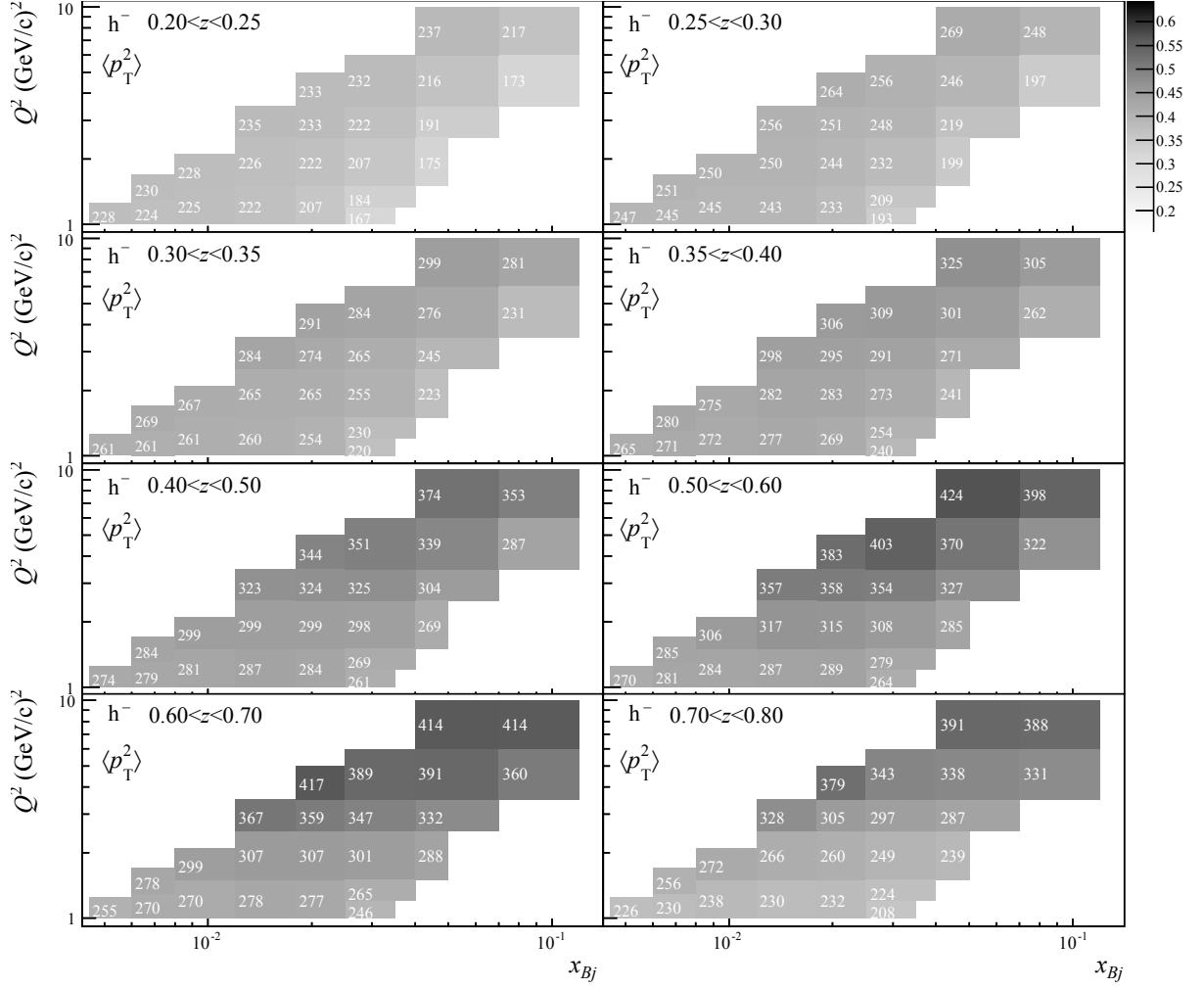


Fig. 6: As Fig. 5 but for negative hadrons.

convoluted with two unintegrated soft universal functions:  $f_q(x_{Bj}, k_\perp)$ , the parton distribution function of quark of flavor  $q$  and  $D_q^h(z, p_\perp)$ , the fragmentation function defined as the number density of hadron  $h$  resulting from the fragmentation of a quark of flavor  $q$ . With the further assumption that both  $f_q(x_{Bj}, k_\perp)$  and  $D_q^h(z, p_\perp)$  follow Gaussian distributions with respect to the transverse momentum variables  $k_\perp$  and  $p_\perp$ , respectively, the cross section can be approximated [16] at first order in  $\mathcal{O}(k_\perp/Q)$  by:

$$\frac{d^4\sigma^{\mu N \rightarrow \mu' h X}}{dx_{Bj} dQ^2 dz dp_T^2} \approx \sum_q \frac{2\pi\alpha^2 e_q^2}{Q^4} f_q(x_{Bj}) D_q^h(z) \cdot [1 + (1-y)^2] \frac{1}{\pi \langle p_T^2 \rangle_q} e^{-p_T^2 / \langle p_T^2 \rangle_q}, \quad (4)$$

where all the parameters describing the transverse momentum dependence of TMDs for a given quark flavor  $q$  are contained in  $\langle p_T^2 \rangle_q$ , through the relation:

$$\langle p_T^2 \rangle_q = \langle p_\perp^2 \rangle_q + z^2 \langle k_\perp^2 \rangle_q. \quad (5)$$

Here again, integration over the azimuthal angle has been performed. In Ref. [16] it was assumed that  $\langle p_\perp^2 \rangle$  and  $\langle k_\perp^2 \rangle$  in Eq. 5 are constants and independent of the quark flavor. In general, they may both depend on  $Q^2$  and the active quark flavor  $q$  while  $\langle p_\perp^2 \rangle$  can depend further on  $z$  and the produced hadron type, and  $\langle k_\perp^2 \rangle$  may depend on  $x_{Bj}$ .

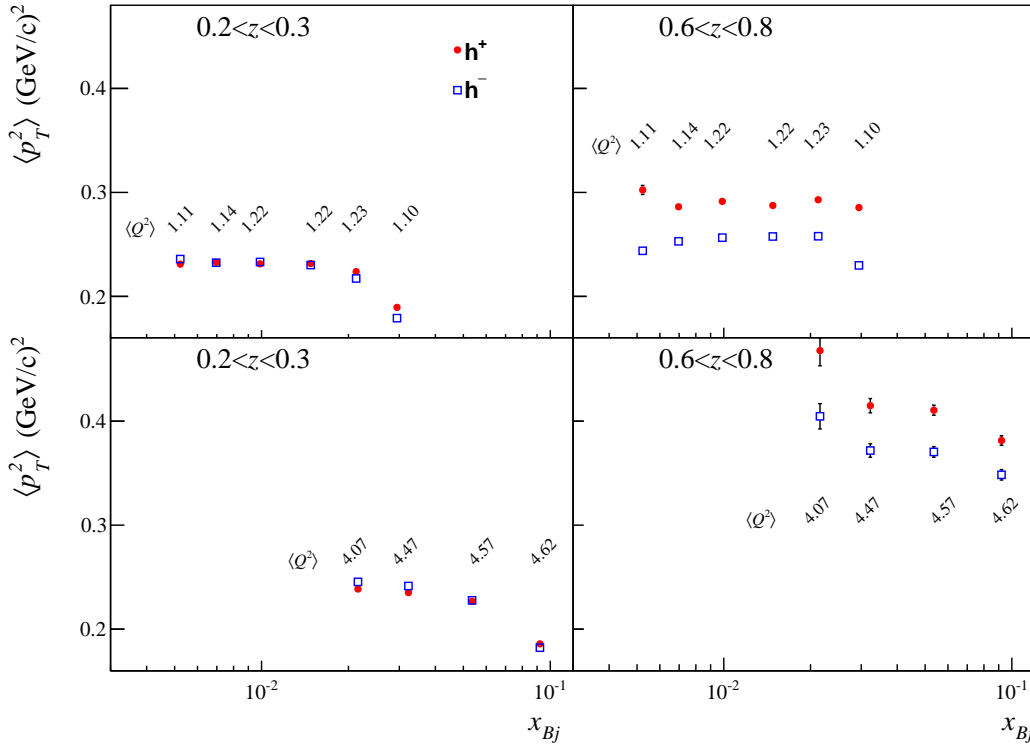


Fig. 7: The fitted  $\langle p_T^2 \rangle$  vs  $x_{Bj}$  for two different  $Q^2$  intervals (top and bottom) and for a low- $z$  bin ( $0.2 < z < 0.3$ ), left, and a high- $z$  bin ( $0.6 < z < 0.8$ ), right, for positive and negative hadrons (red filled circles and blue open boxes). In these figures, the  $\langle p_T^2 \rangle$  values are obtained from a fit over  $0.1 < p_T < 0.85$  GeV/ $c$ . The average value  $\langle Q^2 \rangle$  for each  $x_{Bj}$  bin is indicated.

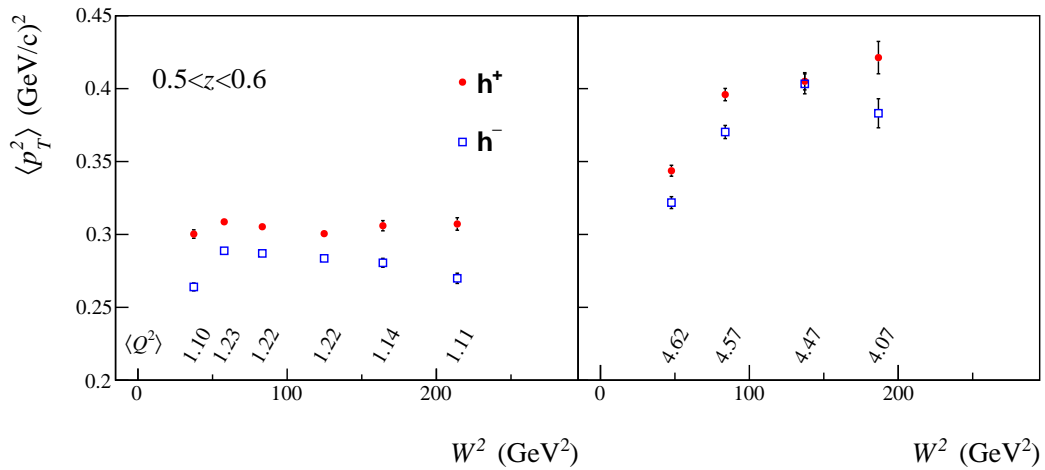


Fig. 8: The fitted  $\langle p_T^2 \rangle$  vs  $W^2$  for  $0.5 < z < 0.6$  and for a low (left) and a high (right)  $Q^2$  interval, from a fit over  $0.1 < p_T$  GeV/ $c < 0.85$ . This is to be compared with Fig. 9 where  $\langle p_T^2 \rangle_{all}$  is plotted. The average  $\langle Q^2 \rangle$  for each  $W^2$  bin are indicated.

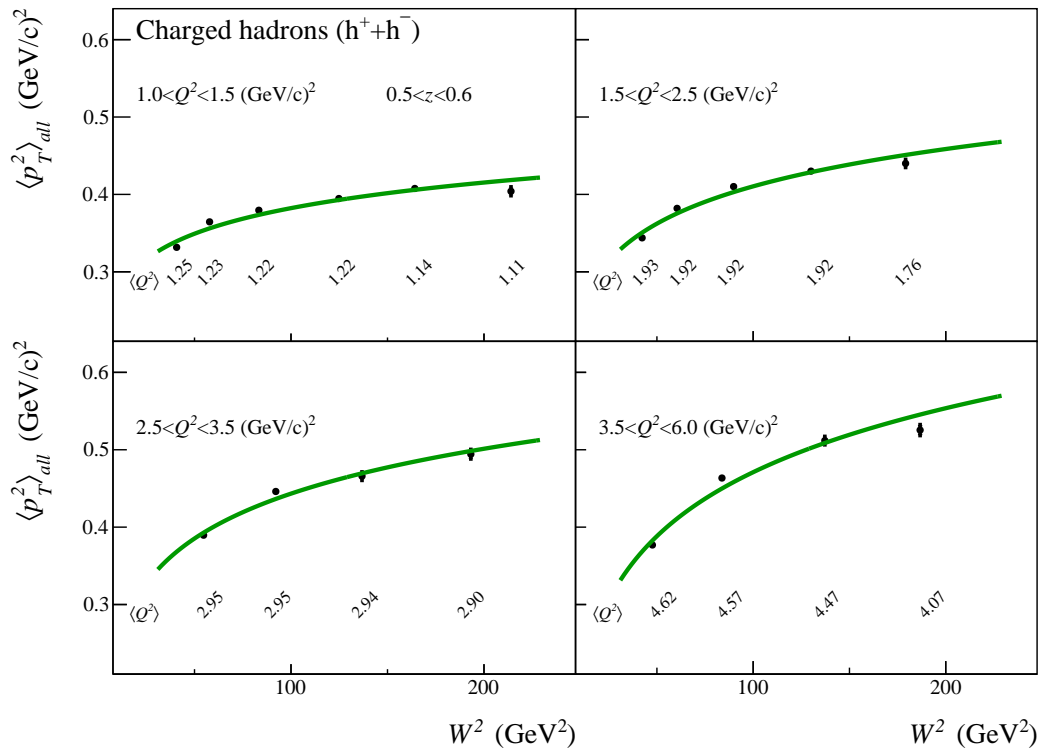


Fig. 9: Statistical average  $\langle p_T^2 \rangle_{all}$  over the entire  $p_T$  range for charged hadrons ( $h^+$  and  $h^-$  summed up) as a function of  $W^2$ , for  $0.5 < z < 0.6$  and four  $Q^2$  intervals, indicated in the figures. The green lines represent fits where a linear function of  $\ln W^2$  was assumed.

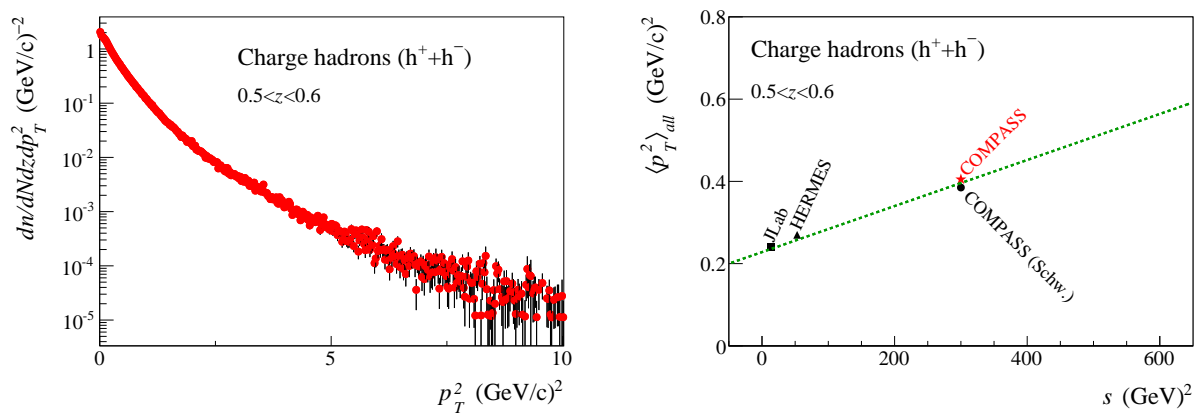


Fig. 10: The  $p_T^2$  distribution of charged hadrons with  $0.5 < z < 0.6$  used to determine the acceptance corrected  $\langle p_T^2 \rangle_{all}$  (left). The  $s$ -dependence of  $\langle p_T^2 \rangle_{all}$  from Ref.[18] (right). The red star labeled COMPASS is the value from this analysis, the black dot labeled COMPASS (Schw.) is the value used in Ref.[18], obtained from data not corrected for acceptance.

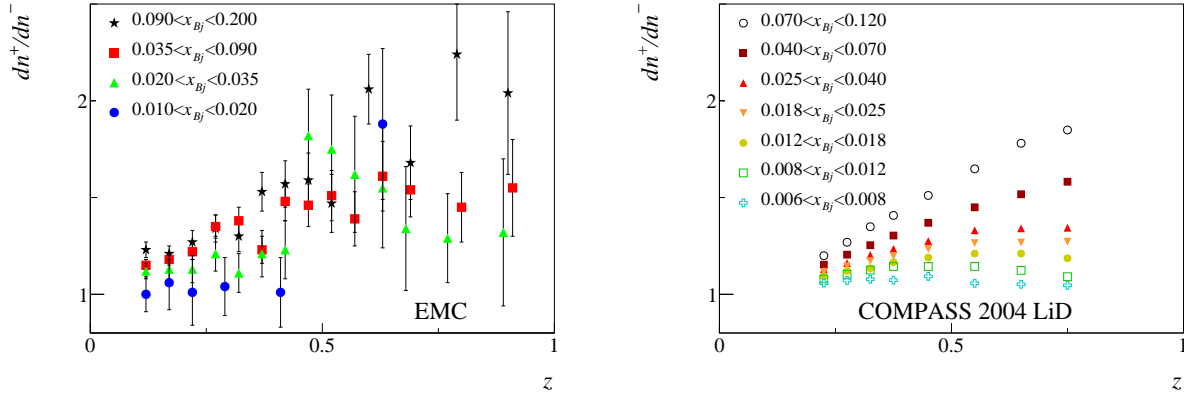


Fig. 11: Charged hadron multiplicity ratios  $dn^{h+}/dn^{h-}$  as a function of  $z$ , for various  $x_{Bj}$  bins, measured by EMC [10] for  $\mu D$  (left) and COMPASS for  $\mu^6\text{LiD}$  (right) interactions respectively. For COMPASS the results are based on part of the 2004 collected statistics.

The observed dependence of the fitted  $\langle p_T^2 \rangle$  on  $z^2$  is shown for two  $(Q^2, x_{Bj})$  intervals in Fig. 12. The relation between  $\langle p_T^2 \rangle$  and  $z^2$  is certainly not linear as in Eq. 5. It should be noted that the non linear behaviour of the  $z^2$ -dependence of  $\langle p_T^2 \rangle$  was reproduced qualitatively in a recent paper [22] by imposing kinematical constraints to the model leading to Eq. 4. A more general ansatz for the contributions of the intrinsic transverse momenta  $p_\perp$  and  $k_\perp$  to the measured hadron transverse momentum  $p_T$  is

$$\langle p_T^2(z) \rangle = \langle p_\perp^2(z) \rangle + z^2 \langle k_\perp^2 \rangle, \quad (6)$$

where  $\langle p_\perp^2(z) \rangle$  is a function of  $z$  and should be taken from other measurements. The dependence of  $k_\perp$  is still the same as in Eq. 6, with a constant average  $\langle k_\perp^2 \rangle$ . The knowledge of  $\langle p_\perp^2(z) \rangle$  could be taken from DIS event generators which are supposed to incorporate all known properties of jet fragmentation. In Fig. 13 the measured values of  $\langle p_T^2 \rangle$  are compared with those of a simulation using the event generator LEPTO<sup>1</sup>. Two cases were simulated in the MC: interactions without intrinsic transverse parton momenta  $\langle k_\perp^2 \rangle = 0$  (open squares) and interactions with  $\langle k_\perp^2 \rangle = 0.25$  (GeV/c)<sup>2</sup> (open crosses). For  $\langle k_\perp^2 \rangle = 0.25$  (GeV/c)<sup>2</sup>, the agreement between  $\langle p_T^2 \rangle$  from simulated events and from data (full squares) is striking for lower values of  $Q^2$ , apart from the highest  $z^2$  bins. For values of  $Q^2$  larger than 4 (GeV/c)<sup>2</sup>, the data are significantly above the simulation. The significant differences between positive and negative hadrons at larger  $z$  values are not reproduced by the MC simulation. This comparison suggests that  $\langle k_\perp^2 \rangle$  can be extracted from the data, provided a detailed tuning of the jet fragmentation parameters would be performed. In addition, it should be noted that the present event selection includes all semi-inclusive events. Thus events which are not due to DIS, i.e. the absorption of the virtual photon by a quark with subsequent quark fragmentation, but to other mechanisms like diffractive vector meson production are included in the sample. The treatment of this kind of background to DIS requires special efforts, in order to extract  $\langle k_\perp^2 \rangle$ .

## 4 Conclusion

The main result of this study is the measurement of differential multiplicities of charged hadrons produced in unpolarised SIDIS of muons off a <sup>6</sup>LiD target. The acceptance corrected multiplicities in a 4-dimensional  $(z, p_T^2, x_{Bj}, Q^2)$  phase space are given in Ref. [15] separately for positively and negatively charged hadrons.

<sup>1</sup>For these simulations, MRST2004LO PDFs in LHAPDF 5.2.2 were used; default LEPTO 6.5.1 and JETSET 7.4 settings, with the exception of LST(11)=122, which includes target mass effects and the longitudinal structure function.

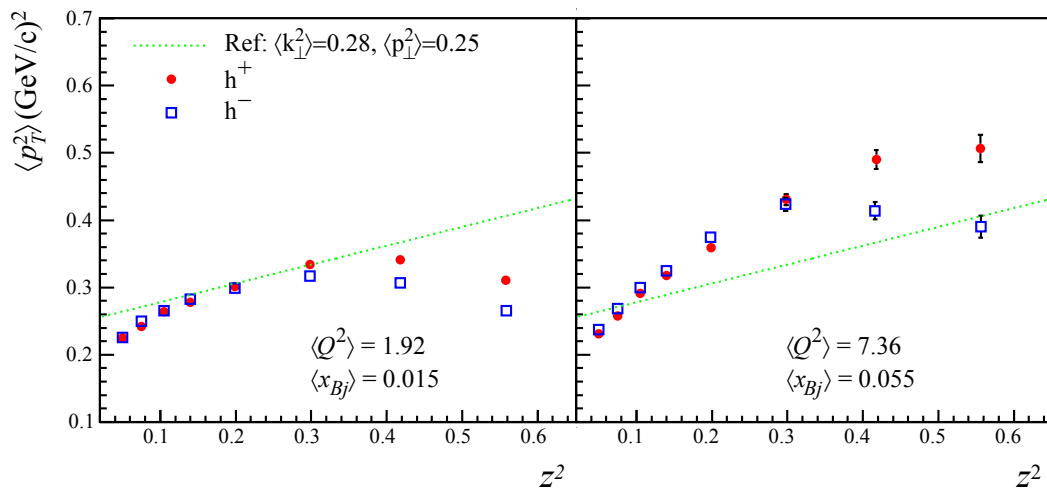


Fig. 12:  $\langle p_T^2 \rangle$  vs  $z^2$  for two  $(Q^2, x_{Bj})$  intervals. The corresponding average values  $\langle Q^2 \rangle$  (in units of  $(\text{GeV}/c)^2$ ) and  $\langle x_{Bj} \rangle$  are indicated in the figure. The dotted green line corresponds to relation (5) with constant  $\langle k_\perp^2 \rangle$  and  $\langle p_\perp^2 \rangle$  from Ref. [17].

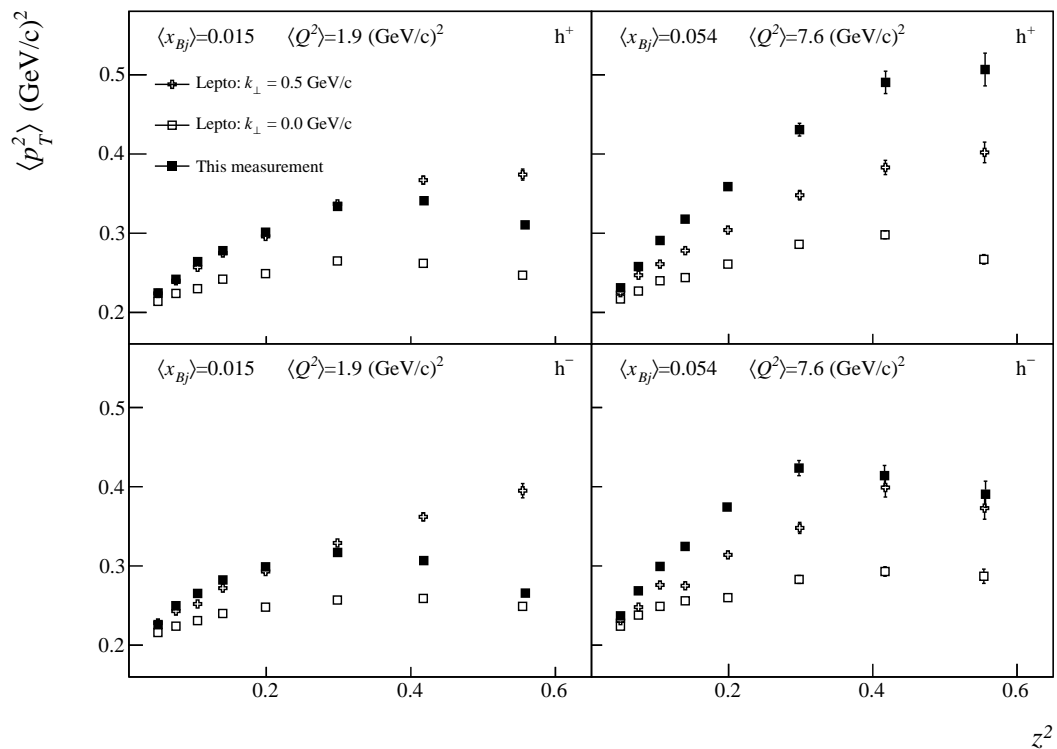


Fig. 13: Comparison of the measured  $\langle p_T^2 \rangle$  (full squares) with a simulation using the MC event generator LEPTO for two bins of  $Q^2$  and  $x_{Bj}$ , for positive (top) and negative hadrons (bottom). Two cases were simulated in the MC: Interactions without intrinsic transverse parton momenta  $\langle k_\perp^2 \rangle = 0$  (open squares) and interactions with  $\langle k_\perp^2 \rangle = 0.25$   $(\text{GeV}/c)^2$  (open crosses).



From these basic multiplicities more complex observables have been extracted. The average  $p_T^2$  over the entire  $p_T$  range,  $\langle p_T^2 \rangle_{all}$ , corrected for acceptance, has been provided for a comparison with other experiments at different center of mass energy. The evolution of  $\langle p_T^2 \rangle_{all}$  as a function of the invariant mass  $W^2$  has been shown to follow a linear dependence on  $\ln W^2$  reasonably well. The ratio of positive over negative hadrons is shown as a function of  $z$  for bins in  $x_{Bj}$  and compared with previous EMC results.

The differential distributions at low  $p_T^2$  have been fitted with an exponential at different  $z$  in order to obtain  $\langle p_T^2 \rangle$ . These data should allow to determine the average intrinsic transverse momentum squared  $\langle k_{\perp}^2 \rangle$  in a framework based on QCD parton model and factorization. The additional information needed to extract  $\langle k_{\perp}^2 \rangle$  is the intrinsic transverse momentum  $\langle p_{\perp}^2 \rangle$  acquired during fragmentation. This information may be derived from up-to-date Monte Carlo simulations like LEPTO or PYTHIA, which incorporate all known properties of jet fragmentation.

This analysis represents the first multidimensional study of hadron multiplicities in unpolarised SIDIS at COMPASS. Further analyses, using the COMPASS ability to identify hadrons, are under way to investigate the production of pions and kaons.

### Acknowledgment

We gratefully acknowledge the support of the CERN management and staff and the skill and effort of the technicians of our collaborating institutes. Special thanks go to V. Anosov and V. Pesaro for their technical support during the installation and the running of this experiment. This work was made possible by the financial support of our funding agencies. We would like to thank Dr. Alessandro Bacchetta for his helpful comments.

### References

- [1] M. Diehl and S. Sapeta, Eur. Phys. J. **C41** (2005) 515
- [2] A. Bacchetta *et al.*, JHEP **0702** (2007) 93.
- [3] R.N. Cahn, Phys. Lett. **B78**, (1978) 269.
- [4] V. Barone, F. Bradamante, and A. Martin, Progr. Part. Nucl. Phys. **65** (2010) 267.
- [5] J.C. Collins, *Foundation of Perturbative QCD*, Cambridge University Press, Cambridge 2011.
- [6] S.M. Aybat and T.C. Rogers, Phys. Rev. **D83** (2011) 114042.
- [7] The CLAS Collaboration, M. Osipenko *et al.*, Phys. Rev. **D80** (2009) 032004; R. Asaturyan *et al.*, Phys. Rev. **C85** (2012) 015202.
- [8] The HERMES Collaboration, A. Airapetian *et al.*, Eur. Phys. J. **C21** (2001) 599 and Phys. Lett. **B684** (2010) 114.
- [9] The E665 Collaboration, M.R. Adams *et al.*, Z. Phys. **C76** (1997) 441.
- [10] The EMC Collaboration, J. Ashman *et al.*, Z. Phys. **C52** (1991) 361.
- [11] J.-F. Rajotte, PhD Thesis at Ludwig Maximilian University Munich, 2010.
- [12] The COMPASS Collaboration, P. Abbon *et al.*, Nucl. Instrum. Meth. **A577** (2007) 455.
- [13] G. Ingelman, A. Edin and J. Rathsmann, Comput. Phys. Commun. **101** (1997) 108.
- [14] See *e.g.* GEANT4 Collaboration, S. Agostinelli *et al.*, Instrum. Meth. A, **506** (2003) 250; J. Allison *et al.*, IEEE Trans. on Nucl. Sci. **53** (2006) 270.

- [15] The Durham HepData Project, <http://hepdata.cedar.ac.uk/reaction>.
- [16] M. Anselmino *et al.*, Phys. Rev. **D71** (2005) 074006.
- [17] M. Anselmino, M. Boglione, A. Prokudin and C. Turk, Eur. Phys. J. **A31** (2007) 373.
- [18] P. Schweitzer, T. Teckentrup A. and Metz, Phys. Rev. **D81** (2010) 094019.
- [19] B. Pasquini and P. Schweitzer, Phys. Rev. **D83** (2011) 114044.
- [20] J.C. Collins, D.E. Soper and G. Sterman, Nucl. Phys. **B250** (1985) 199.
- [21] A. Jgoun on behalf of the HERMES collaboration, Talk given at 36th Rencontres de Moriond on QCD and Hadronic Interactions (2001).
- [22] M. Boglione, S. Melis and A. Prokudin, Phys. Rev. **D84,3** (2011) 034033.
- [23] S. Kretzer, Phys. Rev. **D62** (2000) 054001.
- [24] A. Gawron, J. Kwiecinski and W. Broniowski, Phys. Rev. **D68** (2003) 054001.